Comparative Analysis of Parent and Modified ZSM-5 Zeolites: Insights from Positron Annihilation Lifetime Spectroscopy

Ana Palčić[a], Damir Bosnar[b], Patricija Hršak[c], Josip Bronić[a], Sanja Bosnar[a]*

[a]Ruđer Bošković Institute, Division of Materials Chemistry, Bijenička 51, Zagreb, Croatia
[b]Department of Physics, Faculty of Science, University of Zagreb, Bijenička 32, Zagreb, Croatia
[c]Faculty of Metalurgy, University of Zagreb, Aleja narodnih heroja 3, Sisak, Croatia

E-mail: sbosnar@irb.hr

Abstract

Modified zeolite ZSM-5 samples were prepared by synthesis in the presence of the organics acting as mesoporogens: cationic surfactant, hexadecyltrimethylammonium bromide (CTAB) and cationic polymer, polydiallyldimethylammonium chloride (PDADMAC), as well as by alkali etching of parent zeolite. Properties of modified zeolites were compared to the parent ZSM-5 zeolite. X-ray diffractograms demonstrate that the obtained modified zeolite ZSM-5 samples in all case have preserved parent crystalline zeolite framework of the MFI-type. However, scanning electron micrographs of the same samples show morphology variations of the modified samples as compared to the starting zeolite. Thermogravimetric analyses show distinct weight loss curves of the samples. Differences have been also noted in the OH stretching range of the infrared spectra, and in the results of positron annihilation lifetime spectroscopy (PALS) measurements, which indicated dissimilarities by probing free volume in parent and modified zeolite ZSM-5 samples. In that way, PALS as scarcely used technique in zeolite studies, proved its applicability in structural investigation of this kind.

Keywords

Zeolite ZSM-5, hierarchical, structure, CTAB, PDADMAC, PALS

1. Introduction

Zeolites are crystalline microporous aluminosilicates with pores and cages of uniform sizes and openings. Their main building element is tetrahedron with central T atom and oxygen at vertices. Diverse orientation and linking of tetrahedra via sharing oxygens result in numerous possible zeolite frameworks, majority of them being only theoretically predicted. All-silica zeolites are electrically neutral whereas the insertion of aluminium atoms in the structure brings negative framework charge, which is neutralised by the presence of different exchangeable cations. If the negative charge is compensated by hydrogen, then catalytically active acid site is formed. Such specific porous structure, as well as the presence of silicon and aluminium atoms in different ratios in the framework, makes zeolites very important materials in many different applications like ion-exchange, catalysis, molecular sieving or adsorption (Li and Yu, 2021; Szostak, 1998).

ZSM-5 (Zeolite Socony Mobile-type 5) zeolite belongs to the class of high silica zeolite materials with MFI (Mobil Five) type of structural array and is readily used as a shape selective catalyst in many industrial processes, particularly in oil refining and petrochemical industry (Li and Yu, 2021). MFI structural array is characterized by two sets of perpendicularly intersecting straight and sinusoidal channels, which have elliptic (0.52 x 0.57 nm) and circular (0.53 x 0.56 nm) 10-member ring cross sections, respectively (Szostak, 1998; Derouane and Gabelica, 1980). The catalytic properties of ZSM-5 zeolite are thus based on its three-dimensional framework structure and catalytically active acid sites related to the ratio of silicon to aluminium atoms in the framework. Besides, zeolite ZSM-5 can be synthesized over a wide Si/Al ratio range (Szostak, 1998; Yu et al. 2019, Auepattana-aumrung et al. 2020) which influences number and strength of catalytically active acid sites.

The efficiency of the catalyst as well as the rate of the catalysed reaction is directly correlated to the availability of catalytically active sites to the reactants. Zeolite ZSM-5 is a

highly efficient shape selective catalyst used in processes important in petroleum and petrochemical industry. However, to be applied in the catalytic reactions involving bulkier molecules of reactants or products, i.e., larger than the void dimensions of MFI framework, tailoring of its pore sizes may be required to attain control over the particular catalytic process in terms of the reaction rate as well as the selectivity towards particular product (Primo and Garcia, 2014). One of possible solutions in overcoming such issues is the preparation of hierarchical zeolite material, which, besides standard microporous zeolite structure, possess additional porosity levels, either mesopores or/and macropores (Kerstens et al. 2020). Hierarchical zeolite, then, keeps hydrothermal stability needed for high temperature catalytic reactions as well as catalytic active sites, while on the other side has increased diffusion efficiency and accessibility of those active sites present (Kerstens et al. 2020; Peng et al. 2020).

Miscellaneous procedures for engineering hierarchical zeolites with a wide range of pore sizes have been developed (Li and Yu, 2021; Kerstens et al. 2020; Peng et al. 2020). Generally, hierarchical structure can be formed either during the course of the zeolite synthesis (bottom-up, constructive approach) or by post-synthesis treatments of crystalline material (top-down, destructive approach). During zeolite synthesis, for example, application of different surfactants as soft templates is well known technique used in synthesis of hierarchical zeolites (Park et al. 2011; Zhu et al. 2011; Han et al. 2017; Sabarish and Unnikrishnan 2020; Wang et al. 2021). In addition, different hard templates could be introduced during zeolite synthesis, as for example various carbonaceous materials, biological or polymer materials (Tian et al. 2016; Zhao et al. 2021; Hoang and Thao, 2022). The top-down procedures, which include acid, alkaline or fluoride etching, steaming or irradiation (Groen et al. 2004; Erigoni et al. 2016; Qin et al. 2022) result in removal of aluminium and/or silicon from the zeolite framework, and are also possible ways to tailor zeolite inner structure and availability of acid sites. At the same time, these modifications, particularly the ones occurring during the zeolite synthesis, can

influence not only the inner voids distribution within the zeolite particle and their crystal structure but the morphology of the zeolite crystals as well (Yang et al. 2013; Rimer et al. 2014).

In this work, we modified the porosity degree and the morphology of the parent ZSM-5 zeolite by the synthesis of the parent zeolite ZSM-5 in the presence of mesoporogen agents hexadecyltrimethylammonium bromide (CTAB) and polydiallyldimethyilammonium chloride (PDADMAC) and by the post synthesis treatment by etching parent zeolite ZSM-5 with NaOH solution. The obtained zeolite samples were characterised by X-ray diffraction (XRD), scanning electron microscopy (SEM), thermogravimetric analysis (TGA), infrared spectroscopy (IR) and positron annihilation lifetime spectroscopy (PALS).

2. Experimental

2.1. Synthesis

Chemicals used for the synthesis of parent and modified zeolites were: colloidal silica, (40 wt.% SiO_2 suspension in water, Ludox 40 HS, Grace), aluminium nitrate nonahydrate ($Al(NO_3)_3 \times 9\ H_2O$, 98%, Sigma), sodium hydroxide (NaOH, 98%, Kemika), tetrapropylammonium bromide (TPABr, 98%, Sigma), hexadecyltrimethylammonium bromide (CTAB, 98%, Sigma), polydiallyldimethylammonium chloride (PDADMAC, 20 wt.%, MW 200 000-350 000, Alfa Aesar), distilled water, and were used as obtained.

The parent ZSM-5 zeolite was synthesized after (Ong et al. 2012), from starting precursor gel with molar composition 100 SiO_2 : 0.2 Al_2O_3 : 5 Na_2O : 10 TPABr : 4000 H_2O. Aluminium nitrate nonahydrate was dissolved in appropriate amount of water, subsequently sodium hydroxide was added. In obtained clear solution tetrapropylammonium bromide was added, and finally appropriate amount of silica solution. Reaction mixture prepared in this way was additionally mixed with a magnetic stirrer at RT for an hour to assure homogeneity of the

system. Modified zeolites were synthesized from the same precursor as the parent ZSM-5 zeolite, but in the presence of the CTAB ($CTAB/SiO_2$=0.055) or PDADMAC ($PDADMAC/SiO_2$=0.025). Before adding a modifier, zeolite precursor was aged at 80 °C for one hour. Obtained reaction mixtures were additionally mixed at RT for an hour. All homogenized reaction mixtures were transferred into Teflon lined autoclaves with metal jacket firmly closed and heated at 180 °C for 72 hours. After the synthesis was completed, the obtained white precipitates were washed with copious amount of distilled water and dried at 60 °C overnight. Dried samples were calcined at 550 °C for 5 hours (heating rate 5 °C per minute) in static air atmosphere. The zeolite sample modified by etching was prepared by dispersing dry and calcined parent zeolite in the solution of sodium hydroxide and aluminium nitrate after (Verboekend and Pérez-Ramírez, 2011) for 30 minutes at 65 °C. After etching, the sample was washed with water and dried at 60 °C overnight. All samples, parent and modified, were ion exchanged in NH_4^+ form using 0.5 M NH_4Cl solution two times for 1 hour at 65 °C.

Prepared samples were denoted as follows, parent zeolite: ZSM-5-Parent, etched parent zeolite: ZSM-5-NaOH, parent zeolite synthesized in the presence of CTAB: ZSM-5-CTAB, and parent zeolite synthesized in the presence of PDADMAC: ZSM-5-PDADMAC.

2.2. Characterisation

Dried powder samples were used for characterisation by X-ray diffraction (XRD), thermogravimetric analysis (TG), infrared spectroscopy (IR), scanning electron microscopy (SEM) and positron annihilation lifetime spectroscopy (PALS).

Powder X-ray diffraction patterns of the prepared samples were measured with Malvern Panalytical Aeris Research Edition instrument operating at 40 kV and 7.5 mA using Ni filtered CuKα radiation.

Simultaneous thermal analyser STA 6000 (PerkinElmer, Inc.) was deployed for performing thermogravimetric analysis of the powder samples. Solids were charged in alumina crucibles and heated at rate of 5 °C min^{-1} from room temperature to 800 °C purging at a flow of oxygen gas of 30 mL min^{-1}.

Infrared spectra were acquired using PerkinElmer Fourier transform infrared spectrometer Spectrum Two (PerkinElmer, Inc.) equipped with attenuated total reflexion accessory (FTIR-ATR).

Scanning electron microscopy images were acquired using Tescan MIRA-LMH instrument equipped with a field emission gun.

The positron annihilation lifetime spectroscopy, with ^{22}Na as a positron source sandwiched between the sample tablets, is based on the measurements of the time difference between 1.274 MeV γ-ray, emitted from the daughter ^{22}Ne nucleus almost immediately after positron emission from the ^{22}Na, and one of the annihilated 0.511 MeV γ-rays emitted in annihilation of the positron in the sample. The measurements have been done with modified version of a digitized positron annihilation lifetime spectrometer (Bosnar et al. 2007), which comprises conical BaF_2 scintillators coupled to XP2020 URQ photomultiplier tubes, analog CFDDs (Ortec 583B and FastComTec7029) and digital data acquisition chain with CAMAC TDC (CAEN C414) and ADC (CAEN C205A) units. The source activity was approx. 1 MBq and achieved time resolution in these measurements was about 205 ps.

3. Results and discussion

3.1. X-ray diffraction

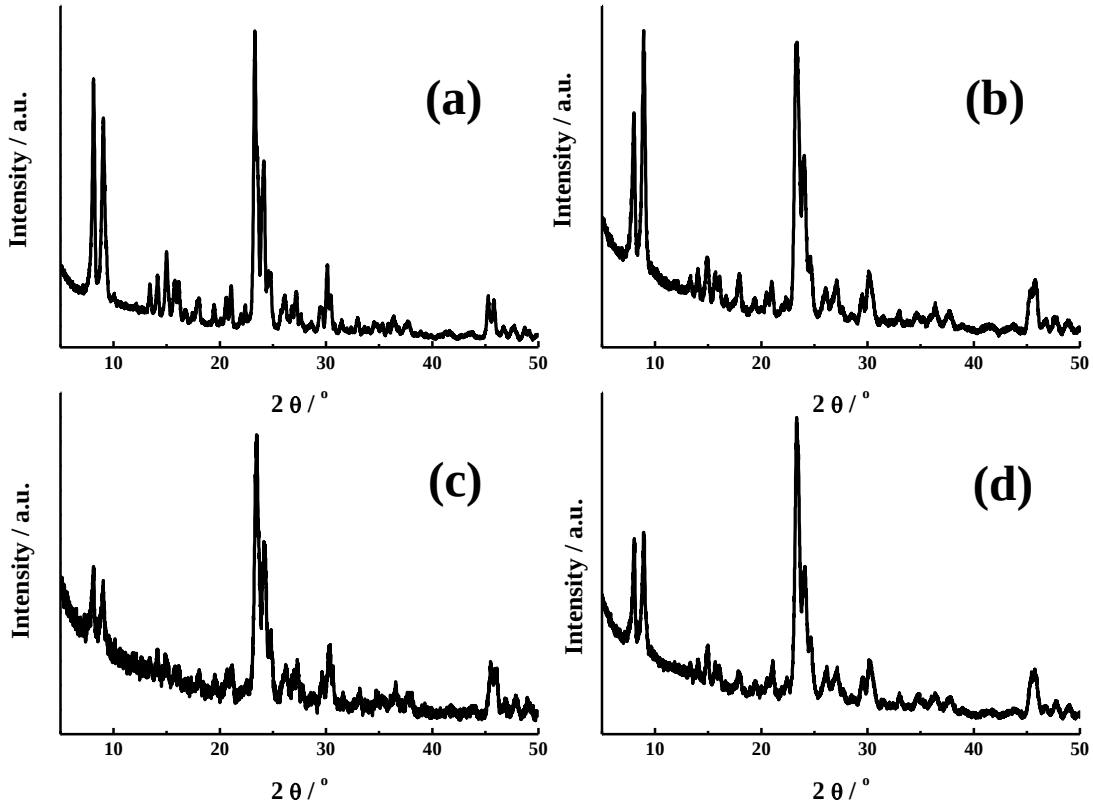

Figure 1. XRD diffractograms of a) ZSM-5-Parent, b) ZSM-5-NaOH, c) ZSM-5-CTAB and d) ZSM-5-PDADMAC.

Results of the XRD characterisation of all four samples are shown in the Figure 1. The diffractograms of all samples are typical for the MFI zeolite structure with characteristic diffraction peaks at 7-9° 2θ and 23-25° 2θ (Treacy and Higgins, 2007). Furthermore, peaks from other structures or the amorphous phase maxima were not detected in diffractogram of any of the characterized samples. Thus, XRD characterisation of the samples shows that the etching of the parent sample has not caused destruction of crystalline zeolite structure in larger extent, and that samples synthesized in the presence of structure modifying agents, ZSM-5-CTAB and ZSM-5-PDADMAC, also represent crystalline zeolite materials of MFI type

structure, although the intensity ratio of characteristic peaks within a particular diffraction pattern is not the same.

3.2. Thermogravimetric analysis

The results of thermogravimetric analysis (TGA) of uncalcined samples are shown in Figure 2 and Table 1. TG curves reveal that weight loss due to removal of water and organic structure directing agents (OSDA) from investigated zeolite samples occurs in a temperature range specific for each sample. Generally, in the weight loss curves of all samples two main regions can be distinguished: a) removal of physically absorbed water (up to 200 ^{o}C for ZSM-5-PDADMAC and ZSM-5-CTAB and up to 350 ^{o}C for ZSM-5-Parent sample) and b) defragmentation, decomposition and degradation of the organic moieties encapsulated within zeolite particles (CTA^{+}, $PDADMA^{n+}$ and TPA^{+}; starting from 200 or 350 °C). Interestingly, in contrast to steep weight loss for parent zeolite, weight decrease of ZSM-5-PDADMAC and especially ZSM-5-CTAB extends over the wider temperature range and the progress seems to be slower due to gentler slope of the curves as well as extra inflection points, i.e. weight loss steps. This behaviour indicates the presence of two distinct organic components occluded within zeolite particles of these samples (Ke et al. 2021).

The weight decrease for samples ZSM-5-CTAB and ZSM-5-PDADMAC (Figures 2b and 2c, Table 1) starts with loss of physically adsorbed water up to 200 ^{o}C, 0.63% and 0.69%, respectively. Further weight loss, from 200 to approximately 360 $^{\circ}$C, of 1.98% and 2.53% for these samples could be connected to the onset of the defragmentation and decomposition CTA^{+} and $PDADMA^{n+}$, respectively (Wang et al. 2010; Chen et al. 2016). The results obtained herein are comparable to the TG measurements reported in different studies of mesoporogen modified zeolite ZSM-5 (Wang, 2010; Moteki, 2014).

On the other hand, a weight loss of 0.58% in the temperature interval from 200 up to 350 °C for the parent zeolite could be due to dehydration (Geus and van Bekkum, 1995) but also to the decomposition of TPA^+ attached to the zeolite crystal surface (Soulard et al., 1987; Milini et al., 2000). Besides its position within MFI structure where it interacts with siloxy groups forming ion pairs, or as counterion balancing negative framework charge in the case of isomorphous substitution of silicon in the framework (Milini et al., 2000), TPA^+ can be, yet in smaller amount, located at the surface of the zeolite crystals involved in the similar interactions as in the interior of the crystal (Soulard et al., 1987). Since TPA^+ is more strongly adhered when within framework, its decomposition starts at higher temperature. Therefore, the weight loss in all samples at temperature range from about 350 °C to 500 °C can be taken mostly as the decomposition of TPA^+ confined within the zeolite voids (Milini et al., 2000; Milanesio et al., 2003). However, in sample ZSM-5-CTAB, degradation of TPA^+ begins at slightly higher temperature and the weight loss is slower with less steep slope compared to parent and ZSM-5-PDADMAC samples, which could be connected to the presence of CTA^+ partially occupying the zeolite channels, slowing down TPA^+ decomposition and removal from the structure (Milini et al., 2000; Milanesio et al., 2003; Xu et al., 2014; Meng et al., 2017). Further weight loss from 500 °C to 700 °C in all samples could be attributed to removal of eventual residues of organic moieties upon decomposition (Wang et al., 2010; Radoor et al., 2021) and/or removal of structural water, i.e., dehydroxylation of silanols (Milini et al., 2000; Chen et al., 2016).

Table 1 shows detailed temperature ranges with respective weight losses and total weight losses for each sample. Higher total weight loss in modified samples as compared to parent sample is in agreement with previous findings and could point, as suggested in literature (Beta et al., 2004; Zhang and Jin, 2011; Sabarish and Unnikrishnan, 2020), to the presence of certain amount of larger pores in the modified samples. Besides, this observation is also in

accordance with the results of positron annihilation lifetime spectra, but this matter is going to be discussed in more details further in the section 3.5.

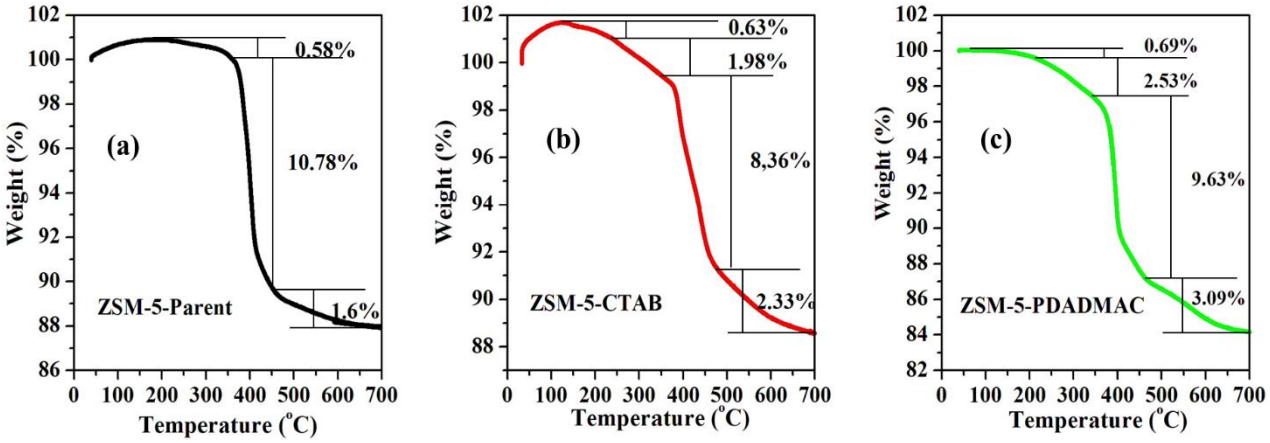

Figure 2. Thermogravimetric analysis (TGA) profiles of a) ZSM-5-Parent, b) ZSM-5-CTAB and c) ZSM-5-PDADMAC.

Table 1. TGA data on the studied samples containing organic moieties.

Temperature range and the respective weight loss amount (wt.%)		
ZSM-5-Parent	**ZSM-5-CTAB**	**ZSM-5-PDADMAC**
200-343 °C (0.58%)	128-227 °C (0.63%)	146-235 °C (0.69%)
343-455 °C (10.78%)	227-370 °C (1.98%)	235-361 °C (2.53%)
455-700 °C (1.6%)	370-502 °C (8.36%)	361-458 °C (9.63%)
	502-700 °C (2.33%)	458-700 °C (3.09%)
Total weight loss 12.96%	Total weight loss 13.3%	Total weight loss 15.94%

3.3. Infrared spectra analysis

Infrared spectra of the of examined zeolite samples, ZSM-5-Parent, ZSM-5-PDADMAC, ZSM-5-CTAB and ZSM-5-NaOH (Figure 3a) are shown in the spectral region from 1400 - 400 cm^{-1}, where appear basic vibrations of the zeolite framework tetrahedra indicating the crystal structure (Flanigen et al., 1974). It can be noticed that lattice vibration modes of all samples are characteristic for MFI zeolite structure, consistent with XRD results (Figure 1). The peak at 1223 cm^{-1} and the broad shoulder at 1060 cm^{-1} can be assigned to the asymmetric stretching vibrations of external T-O linkages and internal tetrahedra (Flanigen et al., 1974), respectively. Furthermore, the peak at 792 cm^{-1} can be attributed to the symmetric stretching of external linkages, while the band at 417 cm^{-1} to the internal T-O bending (Flanigen et al., 1974; Shirazi et al., 2008). Small peak at 627 cm^{-1} can be connected to the vibration of isolated or loosely connected five-membered rings (Lesthaeghe et al., 2008; Airi et al., 2021). The sharp peak at 543 cm^{-1} is characteristic for the vibrations of condensed double five rings in the structure, which is considered as a fingerprint of the MFI structure. This band confirms high crystallinity of the samples in accordance with XRD results (Figure 1) (Serrano et al., 2012). The collected IR spectra indicate nearly identical framework vibrations in the studied parent and modified samples which suggests preservation of the basic zeolite crystal structure, i.e., the long-range ordering, upon modification.

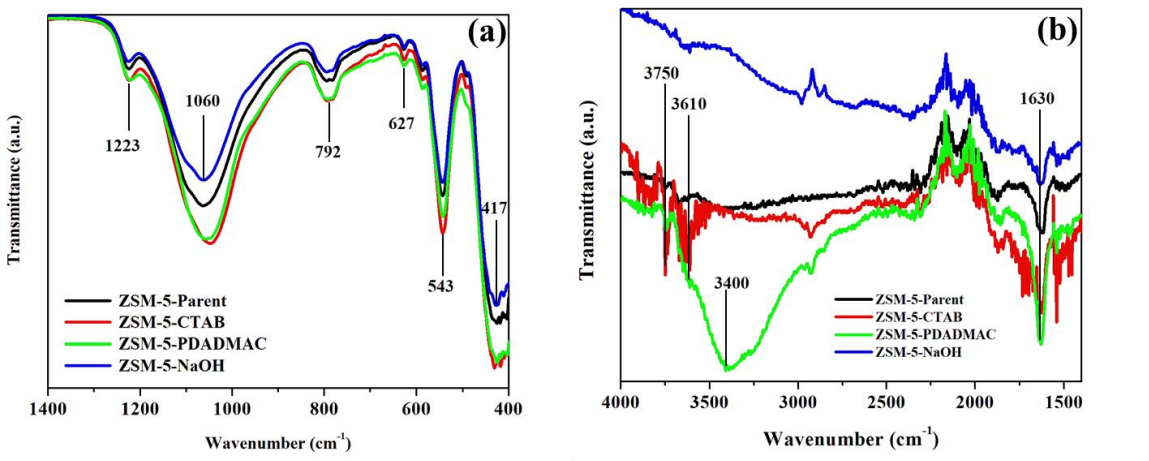

Figure 3. ATR IR spectra of the studied set of samples in the range a) 1400 - 400 cm^{-1} and b) 4000 – 1400 cm^{-1}.

Figure 3b. shows magnified region of the ATR IR spectra from 4000 - 1400 cm^{-1}. The peak at 1630 cm^{-1} is evident in the spectra of all samples, which can be connected to the H-OH bending vibrations of water physisorbed under room temperature conditions confined within microcavities (Wakabayashi et al., 1996; Karbowiak et al., 2010). In hydroxyl stretching vibration region of the spectra, the most prominent is a broad shoulder from about 3200 cm^{-1} to about 3600 cm^{-1} in the ZSM-5-PDADMAC sample spectrum. It is associated with presence of water molecules adsorbed on surface hydroxyl groups and is arising from OH stretching of hydrogen bonded water molecules attached to zeolite surface (Beta et al., 2004; Serrano et al., 2012). Namely, in crystalline zeolite structure the positive charge of the organic cations, here CTA^{+}, $PDADMA^{n+}$ and TPA^{+}, is balanced by siloxy anions, a non-protonated defect sites (Koller et al., 1995); then during calcination and decomposition of organics, siloxy groups get protonated and transform into silanols (Koller et al., 1995; Sano et al., 1997). The higher amount of hydroxyls due to additional pores is therefore expected in mesoporogen modified

zeolites as compared to parent zeolite (Serrano et al., 2012). This observation can be correlated with the TG data where the weight loss arising due to the condensation of silanols is the highest for this very sample (ZSM-5-PDADMAC; range 458-700 °C), once again indicating the highest amount of silanols. However, the absence of broad band at 3200-3600 cm^{-1} in ZSM-5-CTAB, sample and the presence of peaks in the region from 3600-3760 cm^{-1}, which can be related to the presence of free hydroxyl groups on the surface and within pores (Bordiga et al., 2001), could indicate that secondary porosity formed in ZSM-5-PDADMAC differs in terms of position of OH groups in comparison to ZSM-5-CTAB sample. The observed differences likely have origin in specific structure and properties of those large moieties and thus specific interactions each of those have with zeolite precursors during zeolite crystal growth, which results in the formation of more ordered or disordered pores. This finding is in accordance with the other results acquired in this work, i.e., distinct course of thermal degradation for those two samples (Figures 2b and 2c, Table 1), differences in their void sizes distribution and abundance as assessed by PALS (Table 2) as well as in crystal size and morphology documented by SEM micrographs (Figures 4c and 4d).

3.4. Scanning electron microscopy

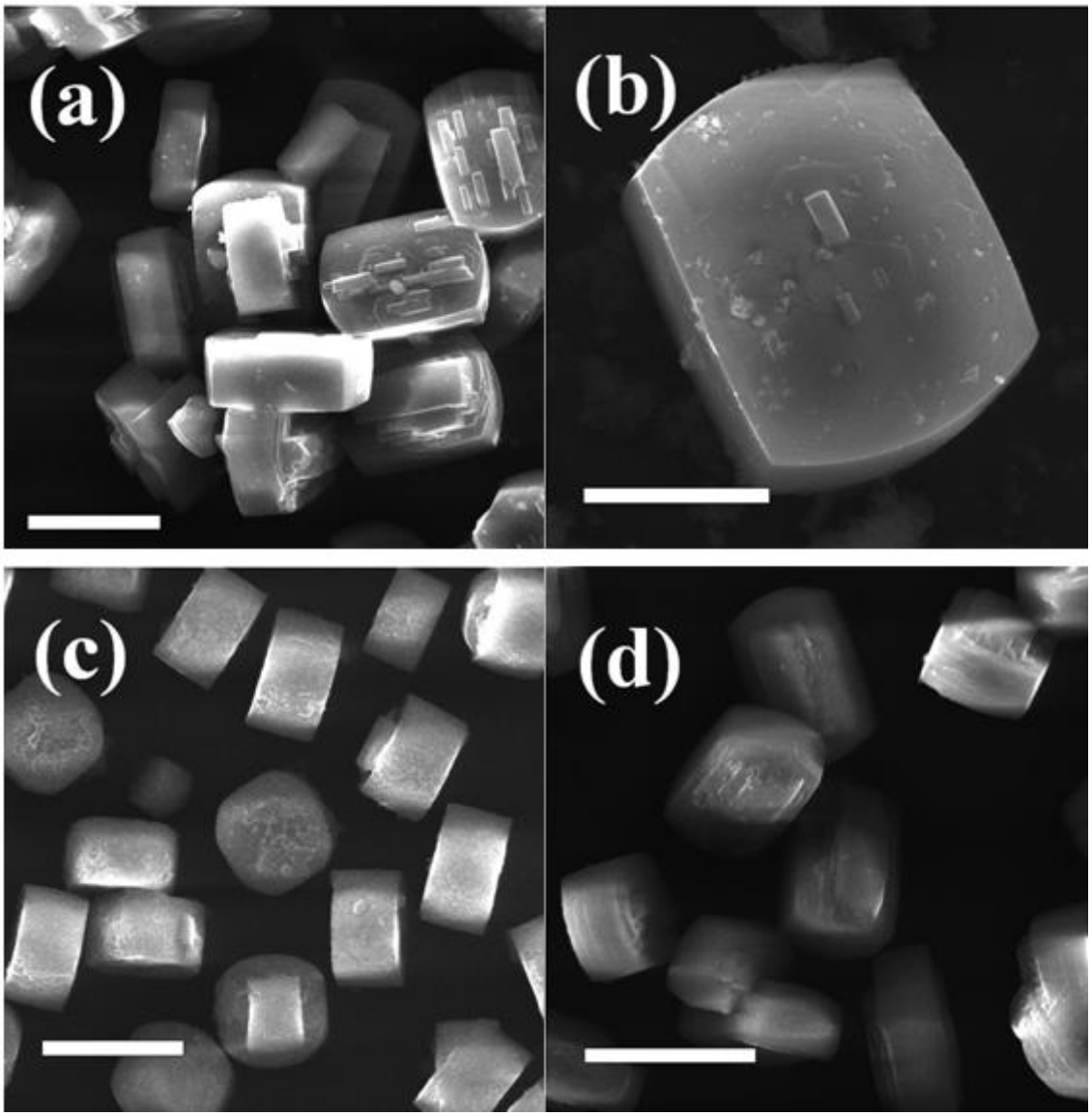

Figure 4. SEM micrographs of a) ZSM-5-Parent, b) ZSM-5-NaOH, c) ZSM-5-CTAB and d) ZSM-5-PDADMAC. Scale bars in a), c) and d) correspond to 20 μm, and in b) to 10 μm.

Morphologies of the investigated samples are assessed on the grounds of the SEM micrographs in Figure 4. Micrograph of the parent zeolite (Figure 4a) shows rounded boat

(coffin shape) twinned crystals with several intergrowths and small ramps and terraces of different sizes formed on the (010) surface of the MFI-type crystal. Intergrown parts are of different size and with sharp edges. Whole crystals have rather uniform size of about 20 to 25 μm.

Representative crystal of the etched sample (ZSM-5-NaOH) is shown in Figure 4b. Some holes on the crystal surface, related to the dissolution/detachment of intergrown crystals are observed. The size of etched crystal is of about 25 μm, implying that applied alkaline treatment has not significantly influenced the sizes of the etched crystals, which remain commensurate to the sizes of the parent zeolite crystals.

The organic molecules used as a mesoporogen in the synthesis of the modified zeolites have different structure. CTAB is amphiphilic surfactant with hydrophilic quaternary ammonium head group and long hydrophobic alkyl chain of 16 C atoms. PDADMAC is on the other hand cationic polymer, large hydrophilic molecule formed by polymerisation of DADMA (diallyldimethylammonium) monomer, which contains charged quaternary ammonium group. Because of hydrophobic tail, CTAB can self-organise into micelles or form hydrophobic interactions with silicate species (Kubota et al., 1996). Opposed to CTAB, PDADMAC molecules do not self-assemble into micelle or other regular structure due to the absence of hydrophobic parts and mesopore that are formed during synthesis are disordered. However, both mesoporogens applied have charged quaternary ammonium groups as a part of molecule, which can act as SDA for the formation of zeolite structure through electrostatic interaction with negative silicate and aluminosilicate species influencing zeolite framework assembly surrounding organic guest molecule (Oliviera et al., 2009). These organic-inorganic interactions strongly affect crystal growth and consequently morphology of the zeolite crystals (Moteki et al., 2014). This impact can be noted also on SEM micrographs of all zeolite samples studied (Figure 4).

Thus, zeolite obtained by synthesis in the presence of CTAB (ZSM-5-CTAB), shown in the Figure 4c, has rather different morphology as compared to the parent zeolite. These crystals have the shape of rounded discs, with sizes of about 15 μm, less twinned/intergrown than the parent sample. Edges of the discs are sharp, but the (010) surface is not smooth; terraces of different heights could be seen. This is in accordance with the finding that since long hydrocarbon chain of the CTA^+ fits into straight channel along *b*-axis (Xu et al., 2014), the crystal growth in that direction is accelerated (Moteki et al., 2014). It is interesting to note that under here applied specific synthesis conditions no separation of phases occurred, i. e. there is only crystalline well shaped material without any amorphous phase. Separation of crystalline and amorphous phase can be rather frequent in the ZSM-5 zeolite synthesis when both CTA^+ and TPA^+ are present as a result of their competitive interaction towards reactive silicate and aluminosilicate species (Zhu et al., 2011; Zhou et al., 2016; Bosnar et al., 2022).

The micrograph in Figure 4d shows crystals of the sample ZSM-5-PDADMAC. The shapes of the crystals are similar to the shape of the parent zeolite crystals (Figure 4a), although intergrowths are larger and more abundant. The main platelets seem to be formed by condensation/stacking of layers of thinner platelets. As it was established earlier, the presence of PDADMAC in the reaction mixture influences viscosity of the system and together with its capping effect interferes growth of platelets and their merging into the crystal (Wang et al., 2013). In the studies of zeolite beta and zeolite ZSM-5 synthesis in the presence of PDADMAC was found that mesopores formed had irregular morphology and connectivity (Wang et al., 2010; Zhu et al., 2014; Tian et al., 2016). The surfaces of crystals in all samples are not smooth, but terraces of different height can be noticed, which could be explained by erroneous incorporation of pentasyl chains and incorporation of the defects in the structure (Agger et al., 2003; Roeffaers et al., 2008). Furthermore, micrographs in Figure 4c and Figure 4d also suggest that the presence of different mesoporogens influences mechanism of zeolite crystal formation

in a different way, depending on the mesoporogen ability to assemble (alumino)silicate species, shape/occupied volume, effective charge, hydrophobicity, etc., which gets reflected in different morphologies of the obtained zeolite crystals (Li et al., 2019).

3.5. Positron annihilation lifetime spectroscopy (PALS)

PALS is a well-known method for structural characterisation of different materials (Puska and Nieminen, 1994; Shantarovich and Goldanski, 1998; Krause-Rehberg and Leipner, 1999; Das et al., 2015; Shi et al., 2018) that provides information on void sizes and their relative concentrations. It is also very suitable for structural characterisation of different porous materials (Shantarovich and Goldanski, 1998; Kobayashi et al., 2007; Novak et al., 2017; van Amelrooij et al., 2020; Bartoš et al., 2021) as well as zeolites (Ito et al., 1999; Consolati et al., 2009; Ferragut et al., 2013; Millina et al., 2015; Bosnar et al., 2017; Chiari et al., 2021). This method is based on the measurement of positron lifetime, from its birth by radioactive decay of radioactive source (i.e., ^{22}Na) to the annihilation by electron inside the structure of the investigated material. Positron lifetime inside porous materials is much longer than in non-porous materials due to the lower electron density inside the voids. When positron enters the sample, it thermalizes in very short time (picoseconds), and depending on the structure of the material, besides direct annihilation with an electron, positron can form a bound state with an electron, called positronium (Ps). Both positron and positronium preferentially reside in empty spaces which have lower electron density (Das et al., 2015; Shi et al., 2018; Li et al., 2019; van Amelrooij et al., 2020). Such empty spaces can be crystal flaws, atomic vacancies, vacancy clusters or micro- and mesoporous voids. The positron and electron of the positronium, can have parallel (called *ortho*-positronium, *o*-Ps) or antiparallel (called *para*-positronium, *p*-Ps) spin orientations, with significantly different lifetimes in vacuum: the *p*-Ps lifetime is approx.

0.125 ns while the *o*-Ps lifetime is approx. 142 ns. However, inside pores of a material *o*-Ps lifetime can vary depending on the structure of material since the positron from *o*-Ps can annihilate with an electron from surrounding material in pick-off process with much shorter lifetime. This provides a solid base for voids size analysis by employing various mathematical models that enable the correlation of *o*-Ps lifetime to the size of pores in which *o*-Ps has annihilated (Tao, 1972; Eldrup et al., 1981; Goworek et al., 1998; Dull et al., 2001; Tanzi Marlotti et al., 2016). Accordingly, it is expected that the *o*-Ps lifetime as well as the amount of the formed *o*-Ps differ in modified zeolite with respect to the non-treated material.

In this study, the lifetime spectra obtained by PALS measurements for investigated samples were fitted by LT v.9, fitting program (Kansy, 1996, 2001). The best fit of annihilation data gives four positron lifetime components for all samples. Associated intensities give information on the relative probability of each component. All lifetime components and the associated intensities with the fitting errors for all samples as well as calculated void sizes are shown in the Table 2.

Table 2. The lifetime values (τ) and the associated intensities (I) with the fitting errors, the effective radii of the voids, R_3 and R_4, calculated by eq. (2) from τ_3 and τ_4, for the samples ZSM-5-Parent, ZSM-5-NaOH, ZSM-5-CTAB and ZSM-5-PDADMAC

Sample	τ_1 / ns I_1 / %	τ_2 / ns I_2 / %	τ_3 / ns I_3 / % R_3 / nm	τ_4 / ns I_4 / % R_4 / nm
ZSM-5-Parent	0.211±0.001 38.7±0.2	0.666±0.002 52.8±0.2	2.78±0.03 3.92±0.04 0.268±0.001	24.4±0.2 4.56±0.03 0.772±0.002
ZSM-5-NaOH	0.197±0.001 30.6±0.2	0.594±0.003 49.1±0.2	3.22±0.02 11.12±0.08 0.293±0.001	9.83±0.06 9.20±0.09 0.519±0.001
ZSM-5-CTAB	0.196±0.001 35.9±0.2	0.552±0.003 39.0±0.2	3.36±0.04 17.8±0.1 0.300±0.001	8.35±0.09 7.4±0.2 0.481±0.002
ZSM-5-PDADMAC	0.217±0.002 40.2±0.3	0.612±0.005 42.0±0.3	3.65±0.04 13.3±0.1 0.314±0.001	16.2±0.2 4.50±0.07 0.649±0.002

The first two lifetime components are usually related to the annihilation of *p*-Ps and free positrons in the bulk of the material, while remaining lifetime components are related to the presence of long-lived *o*-Ps accommodated in larger voids (Kajcsos et al., 2003; Shantarovich et al., 2003; Consolati et al., 2009; Tanzi Marlotti et al., 2016).

Using mathematical models, the lifetime of *o*-Ps can be correlated to the size of voids in which it has had annihilated. Simple Tao-Eldrup model (Tao, 1972; Eldrup et al., 1981) approximates those voids as spheres and it is applicable to the pores with radii smaller than 1 nm:

$$\frac{1}{\tau} = \lambda_b \left[1 - \frac{R}{R+\Delta R} + \frac{1}{2\pi}\sin\left(2\pi \frac{R}{R+\Delta R}\right)\right] \qquad (1)$$

where τ is the *o*-Ps lifetime in ns, R is the void radius in nm, ΔR = 0.166 nm and λ_b = 2 Various extensions of this model aim to explain longer lifetimes and more complex configuration of the voids. Elongated voids characteristic for MFI zeolite structure can be approximated as

cylinders, or cuboids, and the model based on infinite long cylinders can be applied for the correlation of o-Ps lifetimes and sizes of those elongated voids:

$$\frac{1}{\tau} = -2.56 \int_{a_1}^{a_1 \frac{R}{R+\Delta R}} J_0^2(r) r dr \qquad (2)$$

where, J_0 is the cylindrical Bessel function, a_1 is the lowest node of this function and ΔR = 0.166 nm (Jasińska et al., 1996, 1999; Félix et al., 2006).

In all here studied samples the lifetime values of the first components, τ_1, (Table 2) are above vacuum value for *p*-Ps, which is 0.125 ns. Therefore, τ_1 values could be considered as averaged value of the annihilation of *p*-Ps and free positrons in a zeolite bulk (Shantarovich and Goldanski, 1994; Tanzi Marlotti et al., 2016). Likewise, since the lifetimes longer than 0.5 ns suggest presence of *o*-Ps (Mogensen, 1995; Ito et al., 1999; Consolati et al., 2009), the τ_2 values, which for all samples are longer than 0.5 ns (Table 2), can be explained as an average lifetime value of free positron and *o*-Ps lifetime in voids in the bulk structure, like crystal imperfections, vacancies, vacancy clusters, intergrowth or grain boundaries which can act as traps for positron and *o*-Ps (Krause-Rehberg and Leipner, 1999; Tuyen et al., 2017; Shi et al., 2018). Zeolites like other crystalline materials can be abundant in those types of structural defects (Qin et al., 2020). In MFI zeolite structure crystals obtained from highly basic synthesis conditions in the presence of TPABr, as are the synthesis conditions applied also in this study, a complete condensation of zeolite framework is hindered due to specific role of charge balancing of TPA^+ cations (Hunger et al., 1987; Palčić et al., 2022). Besides, prepared MFI zeolite materials could contain some amounts of internal defects generated by the absence of T atoms from the structure. Those defects/voids are covered by silanol groups and can have different size depending on whether they are formed from isolated or clustered T atom vacancies (Bordiga et al., 2000, 2001). On the other hand, as it was proposed in the study of defects in crystalline and amorphous SiO_2 by positron annihilation spectroscopy, regions containing Si-OH species act as traps for positron

and positronium (Fujinami et al., 1993). Therefore, positron and positronium seem to be suitable probe also for these kind of voids/defects in zeolites. The third and the fourth lifetime component obtained by the fit, are related to the presence of *o*-Ps accommodated in at least two types of larger voids, such as regular channels and cages of zeolite structure as well as larger irregular voids in zeolite crystals (Kansy, 1996; Kajcsos et al., 2003; Tanzi Marlotti et al., 2016). Intensity values of *o*-Ps lifetime components are directly correlated to the voids concentration in the matter (Shantarovich and Goldanski, 1998; Ito et al., 1999; Qin et al., 2020; Palčić et al., 2022).

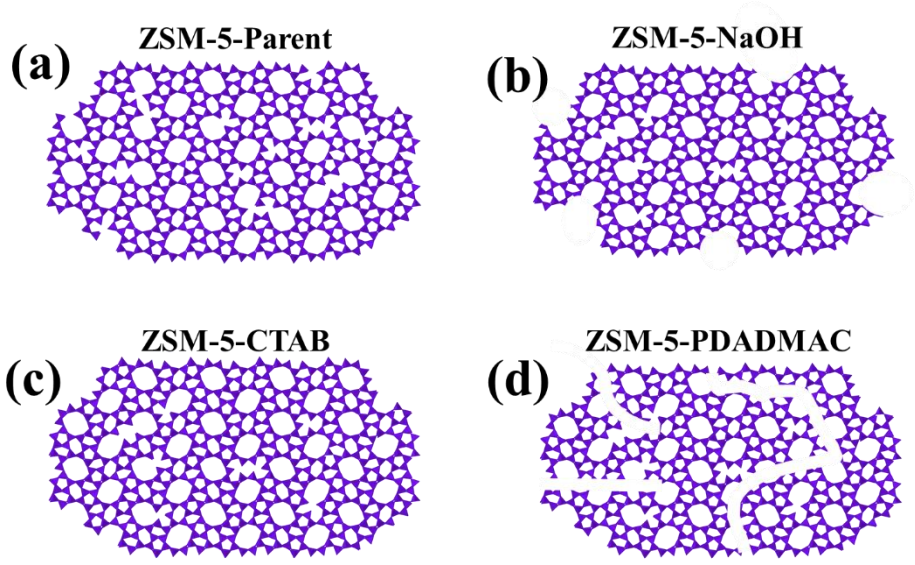

Scheme 1. Simplified representation of the structure of parent and modified samples: a) ZSM-5-Parent, b) ZSM-5-NaOH, c) ZSM-5-CTAB and d) ZSM-5-PDADMAC

Decrease of τ_2 and I_2 values of modified samples compared to the values for ZSM-5-Parent sample (Table 2) suggests that applied modifications influenced also bulk zeolite structure by reducing the size and number of voids in the bulk which can trap free positrons and *o*-Ps. This decrease is the most pronounced for ZSM-5-CTAB sample. As it was mentioned in

previous reports (Moteki et al, 2014; Xu et al., 2014; Meng et al., 2017) the CTA^+ can be accommodated in the MFI framework with long carbohydrate tail in straight channels, and N^+ at intersections of the channels with three methyl groups pointing into straight and sinusoidal channels of the MFI structure. This position is similar to the position of the usual structure directing agent for MFI structure synthesis, TPA^+ cation. However, lower charge density of CTA^+ compared to TPA^+, leads to fewer structural imperfections of the surrounding framework (Moteki et al., 2014). Thus, this modification resulted in less faulted zeolite structure as suggested as well by the decrease of I_2. In the case of the sample ZSM-5-NaOH, it seems that etching removed some smaller voids in the bulk of parent zeolite (slight decrease of τ_2 and I_2 values, Table 2). This decrease could be partially explained by reintegration of eluded as well as externally added aluminium (in etching solution, see subsection 2.1. Synthesis) (Verboekend and Pérez-Ramírez, 2011; da Silva et al., 2019; Peron et al., 2019). Etching also resulted in enlargement of some of the existing zeolite channels, shown by increase in *o*-Ps lifetime and intensities (τ_3, I_3, and τ_4, I_4, sample ZSM-5-NaOH, Table 2). Since the preferential starting points for alkaline etching of zeolite framework are different defect sites (point defects or intergrowth and twinning internal or surface boundaries) (Qin et al., 2020), it is possible that the removal of smaller voids as well as enlargement of zeolite channels occurred by etching of the walls of those small voids/defects placed in the close proximity of the channels or channel intersections (Qin et al., 2021). Decrease in τ_2 value is not as pronounced in ZSM-5-PDADMAC sample. Because of specific structure of $PDADMA^+$ with high density of N^+ moieties, it is reasonable to expect that ZSM-5-PDADMAC sample has high concentration of silanol defects (Koller et al., 1995; Bordiga et al. 2001) creating linear or ring chains (Bordiga et al., 2000) randomly distributed in zeolite structure, which act as traps for positron and *o*-Ps.

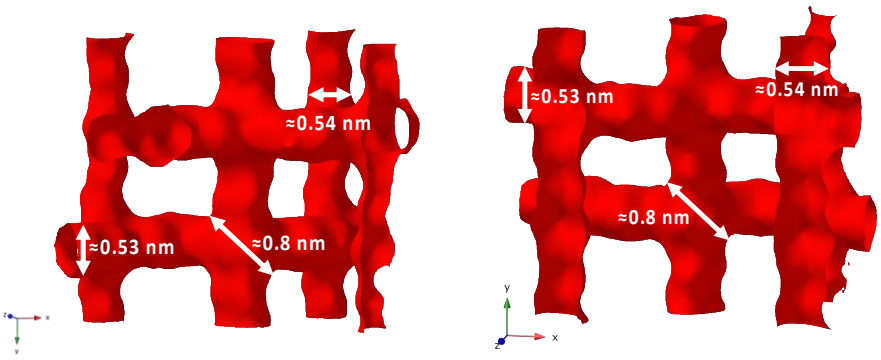

Scheme 2. Approximate dimensions of voids (channels and channel intersections) in MFI-type zeolite framework.

The radius, *R*, of the void calculated from the third component, τ_3, by equation (2) for ZSM-5-Parent sample is 0.268 nm (Table 2), which is in accordance with radius of pores of MFI structure (Scheme 2). The radius of the void calculated from the fourth lifetime component, τ_4, is approximately 0.772 nm (Table 2), which seems rather large value for voids in unmodified MFI structure (Scheme 2). However, since channels of the MFI structure are interconnected there is a possibility for *o*-Ps to diffuse within the channels for longer time. Also, as evidenced by SEM micrographs, parent zeolite crystals have intergrowths and layers at surface. Thus, very large lifetime value of the fourth component, τ_4, could represent the average lifetime of *o*-Ps annihilation in the channels of the crystal and at grain boundaries of intergrowing parts at the surface of the crystal (Svelle et al., 2011; van Amelrooij et al., 2020).

The assignment of radii calculated form the third and fourth lifetime components for modified samples is not so straightforward. In detail, for ZSM-5-NaOH sample radii values R_3 = 0.293 nm and R_4 = 0.519 nm (Table 2) are somewhat larger from the sizes of the channels and channel intersections in MFI structure (Scheme 2) and could represent an averaged value of *o*-Ps annihilation in regular voids (channels and channel intersections) of the MFI zeolite structure and enlarged voids formed by applied modification procedure. Furthermore, for ZSM-

5-CTAB sample calculated R_3 value is 0.3 nm, slightly larger than crystallographic channel sizes, however, R_4 value is 0.481 nm and is close to the size of channel intersections (Scheme 2) (Table 2). As it was discussed previously, due to the lower charge density of CTA^+ this modification resulted in less faulted zeolite structure. In addition, CTA^+ is located within MFI framework with long carbohydrate tail in straight channels and on account of its hydrophobic interactions with surrounding it is possible that there is reduced amount of silanols in the channel walls in this sample. This further could reduce electron density in the channels of ZSM-5-CTAB sample, so less strong interaction of *o*-Ps with the channel walls are the probable reason for its longer lifetime (τ_3, Table 2), related by eq. (2) to higher calculated radii. In the ZSM-5-PDADMAC sample, R_3 and R_4 values, 0.314 nm and 0.649 nm, respectively (Table 2), are the highest of all modified samples and is probably due to mesoporogen function of hydrophilic chain structure of $PDADMA^{n+}$ which results in the formation of random large voids (Table 2). The presumption of the presence of large voids is also in accordance with the highest weight loss as determined by TG analysis (Figure 2 and Table 1).

However, it is important to stress that the sum intensity, $I_3 + I_4$, of long-lived positron component, *o*-Ps, in ZSM-5-Parent sample, is about 8%, while $I_3 + I_4$ sum increases to about 20% for modified samples (Table 2). Considering that *o*-Ps intensity values can be correlated to the number of voids in the studied material (Felix et al., 2002; Cangialosi et al., 2003), the increase of $I_3 + I_4$ sum values in modified samples could be taken as an argument that the modifications of the parent zeolite resulted in enlargement of void space in zeolite structure. However, the sizes of voids are different and depend on the modification processes.

4. Conclusion

Results of this study show that modification of parent zeolite ZSM-5, either by post synthesis treatment or by synthesis in the presence of CTAB and PDADMAC, brings significant changes in the size, morphology and the void distribution of the obtained zeolite crystals. Although significant mesoporosity at applied synthesis/modification conditions has not been achieved, valuable insights in influence of each of modification procedures on the zeolite structure, were established. PALS measurements have demonstrated that besides original microporous network a significant number of larger voids also forms upon these modifications. The amount and size of voids in modified zeolite samples increases, seen by higher lifetime and intensity values of long-lived positron components in comparison to those values in the parent zeolite. This is in agreement with thermogravimetry results where higher weight loss in mesoporogen modified samples are connected to the larger pore volume and more complex porosity. However, in contrast to PDADMAC, the presence of CTAB in the reaction mixture for zeolite ZSM-5 synthesis hinders the formation of flaws. SEM micrographs reveal morphological differences in parent and in modified zeolites. At the same time, XRD diffractograms display, and are corroborated by FT-IR results, that crystal ordering and zeolite structural type has been preserved no matter the treatment as well as that parent and modified zeolites are highly crystalline zeolites of MFI structural type.

Acknowledgements

The authors acknowledge the financial support by the Croatian Science Foundation, under projects IP-2016-06-224, UIP-2019-04-4977; and IAEA CRP F22069 contract 20781.

Authors' contributions

Ana Palčić: Conceptualization, Data curation, Writing-reviewing and editing, Visualisation, Resources, Funding acquisition. **Damir Bosnar**: Investigation, Methodology, Data curation, Formal analysis, Writing-reviewing and editing, Resources, Funding acquisition. **Patricija Hršak**: Formal analysis. **Josip Bronić**: Resources, Funding acquisition. **Sanja Bosnar**: Conceptualisation, Investigation, Formal analysis, Writing-original draft, Visualisation.

Funding

This work was supported by the Croatian Science Foundation [project number: IP-2016-06-224 and project number: UIP-2019-04-4977] and IAEA [CRP F22069 contract 20781].

Competing Interests

The authors declare no competing interests.

References

Airi A.; Signorile M.; Bonino F.; Quagliotto P.; Bordiga S.; Martens J.A.; Crocella V. 2021, Insights on a Hierarchical MFI Zeolite: A Combined Spectroscopic and Catalytic Approach for Exploring the Multilevel Porous System Down to the Active Sites. ACS Appl. Mater. *Interfaces* 13 (41), 49114-49127. https://doi.org/10.1021/acsami.1c11614

Agger J.R.; Hanif N.; Cundy C.S.; Wade A.P.; Dennison S.; Rawlinson P.A.; Anderson M.W. 2003, Silicalite Crystal Growth Investigated by Atomic Force Microscopy. J. Am. Chem. Soc. 125 (3), 830-839. https://doi.org/10.1021/ja020899f

van Amelrooij E.F.; Schut H.; Egger W.; Dickmann M.; Hugenschmidt C.; Mallée L.; Hanefeld U.; McMillan D.G.G.; Eijt S.V.H. 2020, Characterization of Enzymatically Synthesized Titania Thin Films Using Positron Annihilation Spectroscopy Reveals Low-Cost Approach for Organic/Inorganic Photovoltaic Cells. Adv. Sustain. Syst. 4 (6), 2000003 (1-12). https://doi.org/10.1002/adsu.202000003

Auepattana-aumrung C.; Márquez V.; Wannakao S.; Jongsomjit B.; Panpranot J.; Praserthdam P. 2020, Role of Al in Na-ZSM-5 zeolite structure on catalyst stability in butene cracking reaction. Sci. Rep. 10, 13634,1-11. https://doi.org/10.1038/s41598-020-70568-z

Bartoš J.; Šauša O.; Vyroubalová M.; Mat'ko I.; Švajdlenková H. 2021, Confined Effects on Structural Isomers in the MCM-41-SIL Matrix as Seen by Extrinsic Probes via PALS and ESR: n-Butanol vs tert-Butanol. J. Phys. Chem. C 125 (29), 15796-15811. https://doi.org/10.1021/acs.jpcc.1c01951

Beta I.A.; Böhlig H.; Hunger B. 2004, Structure of adsorption complexes of water in zeolites of different types studied by infrared spectroscopy and inelastic neutron scattering. Phys. Chem. Chem. Phys. 6 (8), 1975-1981. https://doi.org/10.1039/B313234J

Bordiga S.; Roggero I.; Ugliengo P.; Zecchina A.; Bolis V.; Artioli G.; Buzzoni R.; Marra G.; Rivetti F.; Spanòd G.; Lambertie C. 2000, Characterisation of defective silicalites. J. Chem. Soc., Dalton Trans. (21), 3921–3929. https://doi.org/10.1039/b004794p

Bordiga S.; Ugliengo P.; Damin A.; Lamberti C.; Spoto G.; Zecchina A.; Spano G.; Buzzoni R.; Dalloro L.; Rivetti F. 2001, Hydroxyls nests in defective silicalites and strained structures

derived upon dehydroxylation: vibrational properties and theoretical modelling. Top. Catal. 15 (1), 43-52. https://doi.org/10.1023/A:1009019829376

Bosnar D.; Kajcsos Z.; Liszkay L.; Lohonyai L.; Major P.; Bosnar S.; Kosanović C.; Subotić B. 2007, Digitized positron lifetime spectrometer for the simultaneous recording of time and energy information. Nucl. Instrum. Meth. A 581 (1-2), 91-93. https://doi.org/10.1016/j.nima.2007.07.035

Bosnar S.; Rac V.; Stošić D.; Travert A.; Postole G.; Auroux A.; Škapin S.; Damjanović-Vasilić Lj.; Bronić J.; Du X.; Marković S.; Pavlović V.; Rakić V. 2022, Overcoming phase separation in dual templating: A homogeneous hierarchical ZSM-5 zeolite with flower-like morphology, synthesis and in-depth acidity study. Microporous Mesoporous Mater. 329, 111534. https://doi.org/10.1016/j.micromeso.2021.111534

Bosnar S.; Vrankić M.; Bosnar D.; Ren N.; Šarić A. 2017, Positron annihilation lifetime spectroscopy (PALS) study of the as prepared and calcined MFI zeolites. J. Phys. Chem. Solids 110, 227-233. https://doi.org/10.1016/j.jpcs.2017.06.016

Cangialosi D.; Schut H.; van Veen A.; Picken S.J. 2003, Positron Annihilation Lifetime Spectroscopy for Measuring Free Volume during Physical Aging of Polycarbonate. Macromolecules 36 (1), 142-147. https://doi.org/10.1021/ma021214z

Chen H.; Wang Y.; Meng F.; Li H.; Wang S.; Sun C.; Wang S.; Wang X. 2016, Conversion of methanol to propylene over nano-sized ZSM-5 zeolite aggregates synthesized by a

modified seed-induced method with CTAB. RSC Adv. 6 (80) 76642-76651. https://doi.org/10.1039/C6RA14753D

Chiari L.; Ohnuki C.; Fujinami M. 2021, Analysis of the Chemical State in Y-zeolite Pores by Positron Annihilation Lifetime Spectroscopy. Anal. Sci. 37 (8), 1117-1122. https://doi.org/10.2116/analsci.20P416

Consolati G.; Mariani M.; Millini R.; Quasso F. 2009, Investigation on the porosity of zeolite NU-88 by means of positron annihilation lifetime spectroscopy. Nucl. Instrum. Meth. B 267 (15), 2550-2553. https://doi.org/10.1016/j.nimb.2009.05.057

Das A.; Mandal A.C.; Roy S.; Nambissan P.M.G. 2015, Positron annihilation studies of defects and fine size effects in nanocrystalline nickel oxide. J. Exp. Nanosci. 10 (8), 622-639. https://doi.org/10.1080/17458080.2013.860490

Derouane E.C.; Gabelica Z.J. 1980, A novel effect of shape selectivity: Molecular traffic control in zeolite ZSM-5. J. Catal. 65 (2), 486-489. https://doi.org/10.1016/0021-9517(80)90328-0

Dull T.L.; Frieze W.E; Gidley D.W.; Sun J.N.; Yee A.F. 2001, Determination of Pore Size in Mesoporous Thin Films from the Annihilation Lifetime of Positronium. J. Phys. Chem. B 105 (20), 4657-4662. https://doi.org/10.1021/jp004182v

Eldrup M.; Lightbody D.; Sherwood J.N. 1981, The temperature dependence of positron lifetimes in solid pivalic acid. Chem. Phys. 63 (1-2), 51-58. https://doi.org/10.1016/0301-0104(81)80307-2

Erigoni A.; Newland S.H.; Paul G.; Marchese L.; Raja R.; Gianotti E. 2016, Creating Accessible Active Sites in Hierarchical MFI Zeolites for Low-Temperature Acid Catalysis. Chem. Cat. Chem. 8 (19), 3161-3169. https://doi.org/10.1002/cctc.201600729

Felix M.V.; Nava R.; Lopez-Castañares R.; Olea-Cardoso O.; Cabral A.; Castaño V.M. 2002, Generalized free volume diagrams from positron annihilation data for the study of nanoporosity in silica gel specimens. Mat. Res. Inovat. 5 (3-4) (2002) 144-150. https://doi.org/10.1007/s10019-002-8639-1

Félix M.V.; Rodríguez-Rojas R.A.; Castañeda-Contreras J.; Nava R.; Consolati G.; Castaño V.M. 2006, Nanoporosity studies of novel catalysts through positronium annihilation. Opt. Mater. 29 (1), 153-157. https://doi.org/10.1016/j.optmat.2006.03.027

Ferragut R.; Aghion S.; Tosi G.; Consolati G.; Quasso F.; Longhi M.; Galarneau A.; Di Renzo F. 2013, Positronium Production in Engineered Porous Silica. J. Phys. Chem. C 117 (50), 26703-26709. https://doi.org/10.1021/jp410221m

Flanigen E.M.; Khatami H.; Szymanski H.A.; Infrared Structural Studies of Zeolite Frameworks. In Molecular Sieve Zeolites-I, Vol. 101; American Chemical Society, 1974; pp 201-229. https://doi.org/10.1021/ba-1971-0101.ch016

Fujinami M.; Chilton N.B.; Ishii K.; Ohki Y. 1993, A positron beam study of defects in SiO2. Journal de Physique IV Colloque 03 (C4), 169-175. https://doi.org/10.1051/jp4:1993423 92

Geus E.R.; van Bekkum H. 1995, Calcination of large MFI-type single crystals, Part 2: Crack formation and thermomechanical properties in view of the preparation of zeolite membranes. Zeolites 15 (4) 333-341. https://doi.org/10.1016/0144-2449(94)00034-P

Goworek T. 2000, Positronium as a Probe of Small Free Volumes. J. Nucl. Radiochem. Sci. 1 (1), 11-13. https://doi.org/10.14494/jnrs2000.1.11

Goworek T; Ciesielski K.; Jasińska B.; Wawryszczuk J. 1998, Positronium states in the pores of silica gel. Chem. Phys. 230 (2-3), 305-315. https://doi.org/10.1016/S0301-0104(98)00068-8

Goworek T.; Jasińska B.; Wawryszczuk J.; Zaleski R.; Suzuki T. 2002, On possible deviations of experimental PALS data from positronium pick-off model estimates. Chem. Phys. 280 (3), 295-307. https://doi.org/10.1016/S0301-0104(02)00491-3

Groen J.C.; Peffer L.A.A.; Moulijn J.A.; Pérez-Ramirez J. 2004, Mesoporosity development in ZSM-5 zeolite upon optimized desilication conditions in alkaline medium. Colloids Surf. A Physicochem. Eng. Asp. 241 (1-3), 53-58. https://doi.org/10.1016/j.colsurfa.2004.04.012

Han S.W.; Kim J.; Ryoo R. 2017, Dry-gel synthesis of mesoporous MFI zeolite nanosponges using a structure-directing surfactant. Microporous Mesoporous Mater. 240, 123-129. https://doi.org/10.1016/j.micromeso.2016.11.016

Hoang P.H.; Thao N.T.T. 2022, Dry gel synthesis of hierarchical ZSM-5 zeolite using hydroxyl propyl methyl cellulose (HPMC) as a mesoporogen and its catalytic activity in alkylation reactions. RSC Adv. 12 (38), 24511-24517. https://doi.org/10.1039/D2RA04325D

Hunger M.; Kärger J.; Pfeifer H.; Caro J.; Zibrowius B.; Bülow M.; Mostowicz R. 1987, Investigation of internal silanol groups as structural defects in ZSM-5-type zeolites. J. Chem. Soc., Faraday Trans. 83 (11), 3459-3468. https://doi.org/10.1039/F19878303459

Ito K.; Yagi Y.; Hirano S.; Miyayama M.; Kudo T.; Kishimoto A.; Ujihira Y. 1999, Estimation of Pore Size of Porous Materials by Positron Annihilation Lifetime Measurement. J. Cer. Soc. Jpn. 107 (2) 123-127. https://doi.org/10.2109/jcersj.107.123

Jasińska B.; Kozioł A.E.; Goworek T. 1996, Ortho-positronium lifetimes in nonspherical voids. J. Radioanal. Nucl. Chem. 210 (2), 617-623. https://doi.org/10.1007/BF02056403

Jasińska B.; Koziol A.E.; Goworek T. 1999, Void Shapes and o-Ps Lifetime in Molecular Crystals. Acta Phys. Pol. A 95 (4), 557-561. https://doi.org/10.12693/APhysPolA.95.557

Kajcsos Zs.; Liszkay L.; Duplâtre G.; Lohonay L.; Varga L.; Lazar K.; Pál-Borbély G.; Beyer H.K.; Caullet P.; Patarin J.; de Lima A.P.; Lopes Gil C.; Gordo P.M.; Ferreira Marques M.F. 2003, Positron and positronium in porous media: zeolites. Radiat. Phys. Chem. 68 (3-4), 363-368. https://doi.org/10.1016/S0969-806X(03)00185-3

Kansy J. 1996, Microcomputer program for analysis of positron annihilation lifetime spectra. Nucl. Instrum. Meth. A 374 (2), 235-244. https://doi.org/10.1016/0168-9002(96)00075-7

Kansy J. 2001, Programs for Positron Lifetime Analysis Adjusted to the PC Windows Environment. Mater. Sci. Forum 363-365, 652-654. https://doi.org/10.4028/www.scientific.net/MSF.363-365.652

Karbowiak T.; Saada M-A.; Rigolte S.; Ballandras A.; Weber G.; Bezverkhyy I.; Soulard M.; Patarin J.; Bellat J-P. 2010, New insights in the formation of silanol defects in silicalite-1 by water intrusion under high pressure. Phys. Chem. Chem. Phys. 12 (37), 11454-11466. https://doi.org/10.1039/C000931H

Ke Q.; Khalil I.; Smeyers B.; Li Z.; de Oliveira-Silva R.; Sels B.; Sakellariou D.; Dusselier M. A 2021, Cooperative OSDA Blueprint for Highly Siliceous Faujasite Zeolite Catalysts with Enhanced Acidity Accessibility. Angew. Chem. Int. Ed. 60 (45), 24189–24197. https://doi.org/10.1002/anie.202109163

Kerstens D.; Smeyers B.; Van Waeyenberg J.; Zhang Q.; Yu J.; Sels B.F. 2020, State of the Art and Perspectives of Hierarchical Zeolites: Practical Overview of Synthesis Methods and Use in Catalysis. Adv. Mater. 32 (44), 2004690, 1-47. https://doi.org/10.1002/adma.202004690

Kobayashi Y.; Ito K.; Oka T.; Hirata K. 2007, Positronium chemistry in porous materials. Radiat. Phys. Chem. 76 (2), 224-230. https://doi.org/10.1016/j.radphyschem.2006.03.042

Koller H.; Lobo R.F.; Burkett S.L.; Davis M.E. 1995, SiO-.cntdot. .cntdot. .cntdot.HOSi Hydrogen Bonds in As-Synthesized High-Silica Zeolites. J. Phys. Chem. 99 (33), 12588-12596. https://doi.org/10.1021/j100033a036

Krause-Rehberg R.; Leipner H.S.; Positron Annihilation in Semiconductors: Defect Studies; Springer,1999

Kubota Y.; Helmkamp M.M.; Zones S.I.; Davis M.E. 1996, Properties of organic cations that lead to the structure-direction of high-silica molecular sieves. Microporous Mater. 6 (4), 213-229. https://doi.org/10.1016/0927-6513(96)00002-8

Lesthaeghe D.; Vansteenkiste P.; Verstraelen T.; Ghysels A.; Kirschhock C.E.A.; Martens J.A.; Van Speybroek V.; Waroquier M. 2008, MFI Fingerprint: How Pentasil-Induced IR Bands Shift during Zeolite Nanogrowth. J. Phys. Chem. C 112 (25), 9186-9191. https://doi.org/10.1021/jp711550s

Li Y.; Yu J. 2021, Emerging applications of zeolites in catalysis, separation and host–guest assembly. Nat. Rev Mater. 6, 1156-1174. https://doi.org/10.1038/s41578-021-00347-3

Li S.; Li J.; Dong M.; Fan S.; Zhao T.; Wang J.; Fan W. 2019, Strategies to control zeolite particle morphology. Chem. Soc. Rev. 48 (3), 885-907. https://doi.org/10.1039/C8CS00774H

Meng L.; Mezari B.; Goesten M.G.; Hensen E.J.M. 2017, One-Step Synthesis of Hierarchical ZSM-5 Using Cetyltrimethylammonium as Mesoporogen and Structure-Directing Agent. Chem. Mater. 29 (9), 4091-4096. https://doi.org/10.1021/acs.chemmater.7b00913

Milanesio M.; Artioli G.; Gualtieri A.F.; Palin L; Lamberti C. 2003, Template Burning inside TS-1 and Fe-MFI Molecular Sieves: An in Situ XRPD Study. J. Am. Chem Soc. 125 (47) 14549-14558. https://doi.org/10.1021/ja037229+

Milina M.; Mitchell S.; Cooke D.; Crivelli P.; Pérez-Ramírez J. 2015, Impact of Pore Connectivity on the Design of Long-Lived Zeolite Catalysts. Angew. Chem., Int. Ed. 54 (5), 1591-1594. https://doi.org/10.1002/anie.201410016

Milini R.; Perego G.; Berti D.; Parker Jr. W.O.; Carati A.; Bellussi G. 2000, Structural characterization of as-synthesized B- and Ti-containing MFI-type molecular sieves. Microporous Mesoporous Mater. 35-36, 387-403. https://doi.org/10.1016/S1387-1811(99)00236-X

Mogensen O.E., Positron Annihilation in Chemistry, Springer-Verlag, 1995. https://doi.org/10.1007/978-3-642-85123-0

Moteki T.; Keoh S.H.; Okubo T. 2014, Synthesis of zeolites using highly amphiphilic cations as organic structure-directing agents by hydrothermal treatment of a dense silicate gel. Chem. Commun. 50 (11), 1330—1333. https://doi.org/10.1039/C3CC48396G

Novak S.; Singh V.; Monmeyran C.; Ingram A.; Han Z.; Lin H.; Borodinov N.; Patel N.; Du Q.; Hu J.; Luzinov I.; Golovchak R.; Agarwal A.; Richardson K. 2017, Positron annihilation lifetime spectroscopy (PALS) studies of gamma irradiated As2Se3 films used in MIR integrated photonics. J. Non-Cryst. Solids 455, 29-34. https://doi.org/10.1016/j.jnoncrysol.2016.10.021

Oliviera A.C.; Martinis L.; Cardoso D. 2009, Basic catalytic properties of as-synthesized molecular sieves. Microporous Mesoporous Mater. 120 (3), 206-213. https://doi.org/10.1016/j.micromeso.2008.10.033

Ong L.H.; Dömök M.; Olindo M.R.; van Veen A.C.; Lercher J.A. 2012, Dealumination of HZSM-5 via steam-treatment. Microporous Mesoporous Mater. 164, 9-20. https://doi.org/10.1016/j.micromeso.2012.07.033

Palčić A.; Moldovan S.; El Siblani H.; Vicente A.; Valtchev V. 2022, Defect Sites in Zeolites: Origin and Healing. Adv. Sci. 9 (4), 2104414 (1-11). https://doi.org/10.1002/advs.202104414

Park W.; Yu D.; Na K.; Jelfs K.E.; Slater B.; Sakamoto Y.; Ryoo R. 2011, Hierarchically Structure-Directing Effect of Multi-Ammonium Surfactants for the Generation of MFI Zeolite Nanosheets. Chem. Mater. *23* (23), 5131-5137. https://doi.org/10.1021/cm201709q

Peng P.; Gao X-H.; Yan Z-F.; Mintova S. 2020, Diffusion and catalyst efficiency in hierarchical zeolite catalysts. Natl. Sci. Rev. 7 (11), 1726-1742. https://doi.org/10.1093/nsr/nwaa184

Peron D.V.; Zholobenko V. L.; de Melo J. H. S.; Capron M.; Nuns N.; de Souza M. O.; Feris L.A.; Marcilio N.R.; Ordomsky V.V.; Khodakov A.Y. 2019, External surface phenomena in dealumination and desilication of large single crystals of ZSM-5 zeolite synthesized from a sustainable source. Microporous Mesoporous Mater. 286, 57-64. https://doi.org/10.1016/j.micromeso.2019.05.033.

Primo A.; Garcia H. 2014, Zeolites as catalysts in oil refining. Chem. Soc. Rev. *43*, 7548 - 7561. https://doi.org/10.1039/C3CS60394F

Puska M.J.; Nieminen R.M. 1994, Theory of positrons in solids and on solid surfaces. Rev. Mod. Phys. 66 (3), 841-897. https://doi.org/10.1103/RevModPhys.66.841

Qin Z.; Hafiz L.; Shen Y.; Van Daele S.; Boullay P.; Ruaux V.; Mintova S.; Gilson J-P.; Valtchev V. 2020, Defect-engineered zeolite porosity and accessibility. J. Mater. Chem. A, 8 (7), 3621-3631. https://doi.org/10.1039/c9ta11465c

Qin Z.; You Z.; Bozhilov K.N.; Kolev S.K.; Yang W.; Shen Y.; Jin X.; Gilson J-P.; Mintova S.; Vayssilov G.N.; Valtchev V. 2022, Dissolution Behavior and Varied Mesoporosity of Zeolites by NH4F Etching. Chem. Eur. J. 28 (16), e202104339, 1-7. https://doi.org/10.1002/chem.202104339

Qin Z.; Zeng S.; Melinte G.; Bučko T.; Badawi M.; Shen Y.; Gilson J-P.; Ersen O.; Wei Y.; Liu Z.; Liu X.; Yan Z.; Xu S.; Valtchev V.; Mintova S. 2021, Understanding the Fundamentals of Microporosity Upgrading in Zeolites: Increasing Diffusion and Catalytic Performances. Adv. Sci. 8 (17), 2100001 (1-9). https://doi.org/10.1002/advs.202100001

Radoor S.; Karayil J.; Jayakumar A.; Parameswaranpillai J.; Siengchin S. 2021, Removal of Methylene Blue Dye from Aqueous Solution using PDADMAC Modified ZSM-5 Zeolite as a Novel Adsorbent. J. Polym. Environ. 29 (10), 3185-3198. https://doi.org/10.1007/s10924-021-02111-8

Rimer J.D.; Kumar M.; Li R.; Lupulescu A.I.; Oleksiak M.D. 2014, Tailoring the physicochemical properties of zeolite catalysts. Catal. Sci. Technol. 4 (11), 3762-3771. https://doi.org/10.1039/C4CY00858H

Roeffaers M.B.J.; Ameloot R.; Baruah M.; Uji-I H.; Bulut M.; De Cremer G.; Müller U.; Jacobs P.A.; Hofkens J.; Sels B.F.; De Vos D.E. 2008, Morphology of Large ZSM-5 Crystals Unraveled by Fluorescence Microscopy. J. Am. Chem. Soc. 130 (17), 5763-5772. https://doi.org/10.1021/ja7113147

Sabarish R.; Unnikrishnan G. 2020, A novel anionic surfactant as template for the development of hierarchical ZSM-5 zeolite and its catalytic performance. J. Por. Mater. 27 (3), 691-700. https://doi.org/10.1007/s10934-019-00852-5

Sano T.; Ikeya H.; Kasuno T.; Wang Z.B.; Kawakami Y.; Soga K. 1997, Influence of Crystallinity of HZSM-5 Zeolite on Its Dealumination Rate. Zeolites 19 (1), 80-86. https://doi.org/10.1016/S0144-2449(97)00052-3

Serrano D.P.; Sanz R.; Pizzaro P.; Moreno I. 2012, Tailoring the properties of hierarchical TS-1 zeolite synthesized from silanized protozeolitic units. Appl. Cat. A 435-436, 32-42. https://doi.org/10.1016/j.apcata.2012.05.033

Shantarovich V.P.; Goldanski V.I. 1998, Positron annihilation in free volume elements of polymer structures. Hyperfine Interactions, 116 (1-4), 67-81. https://doi.org/10.1023/A:1012622822148

Shantarovich V.P.; Suzuki T.; He C. 2003, A possibility to study the properties of substances using positronium as the simplest "labeled" atom. J. Radioanal. Nucl. Chem., 255, 165-170. https://doi.org/10.1023/A:1022208604628.

Shirazi L.; Jamshidi E.; Gasemi M.R. 2008, The effect of Si/Al ratio of ZSM-5 zeolite on its morphology, acidity and crystal size. Cryst. Res. Technol. 43 (12), 1300-1306. https://doi.org/10.1002/crat.200800149

Shi W.; Theelen M.; Illiberi A.; Barreau N.; van der Sar S.J.; Butterling M.; Schut H.; Egger W.; Dickmann M.; Hugenschmidt C.; Zeman M.; Brück E.; Eijt S.V.H. 2018, Evolution and role of vacancy clusters at grain boundaries of ZnO: Al during accelerated degradation of Cu(In, Ga)Se_2 solar cells revealed by positron annihilation. Phys. Rev. Mater. 2 (10), 105403. https://doi.org/10.1103/PhysRevMaterials.2.105403

da Silva L.S.; Akemi Araki C.; Parmegiani Marcucci S.M.; dos Santos Teixeira da Silva L.V; Arroyo P.A. 2019, Desilication of ZSM-5 and ZSM-12 Zeolites with Different Crystal Sizes:

Effect on Acidity and Mesoporous Initiation. Materials Research. 22 (2), e20180872 (1-9). https://doi.org/10.1590/1980-5373-MR-2018-0872

Soulard M.; Biliger S.; Kessler H.; Guth J.L. 1987, Thermoanalytical characterization of MFI-type zeolites prepared either in the presence of OH− or of F− ions. Zeolites 7 (5), 463-470. https://doi.org/10.1016/0144-2449(87)90016-9

Svelle S.; Sommer L.; Barbera K.; Vennestrøm P.N.R.; Olsbye U.; Lillerud K.P.; Bordiga S.; Pan Y-H.; Beato P. 2011, How defects and crystal morphology control the effects of desilication. Catal. Today 168 (1), 38–47. https://doi.org/10.1016/j.cattod.2010.12.013

Szostak R., Molecular Sieves; Blackie Academic & Professional, 1998. https://doi.org/10.1002/(SICI)1099-0739(199903)13:3<209::AID-AOC817>3.0.CO;2-P

Tao S.J. 1972, Positronium Annihilation in Molecular Substances. J. Chem. Phys. 56 (11), 5499-5510. https://doi.org/10.1063/1.1677067

Tanzi Marlotti G.; Castelli F.; Consolati G. 2016, Positronium Confinement in Small Cavities: A Two-Particle Model for the Lowering of Contact Density. Phys.Rev.Lett. 116 (3), 033401. https://doi.org/10.1103/PhysRevLett.116.033401

Tian Q.; Liu Z.; Zhu Y.; Dong X.; Saih Y.; Basset J-M.; Sun M.; Xu W.; Zhu L.; D.Zhang D.; Huang J.; Meng X.; Xiao F-S.; Han Y. 2016, Beyond Creation of Mesoporosity: The Advantages of Polymer-Based Dual-Function Templates for Fabricating Hierarchical Zeolites. Adv. Funct. Mater. *26* (12), 1881-1891. https://doi.org/10.1002/adfm.201504888

Treacy M.M.J.; Higgins J.B.; Collection of Simulated XRD Powder Patterns for Zeolites, Elsevier, 2007. https://doi.org/10.1016/B978-0-444-53067-7.X5470-7

Tuyen L.A.; Hung N.Q.; Cuong L.C.; Khiem D.D.; Phuc P.T.; Nguyen L.L.; Hue N.T.N.; Hue P.T.; Phuc D.V. 2017, Simultaneous existence of defects and mesopores in nanosized ZSM-5 zeolite studied by positron annihilation and X-ray diffraction spectroscopies. J. Appl. Phys. 2017, 121 (8), 084303. https://doi.org/10.1063/1.4977013

Verboekend D.; Pérez-Ramírez J. 2011, Desilication Mechanism Revisited: Highly Mesoporous All-Silica Zeolites Enabled Through Pore-Directing Agents. Chem. Eur. J. 17 (4), 1137-1147. https://doi.org/10.1002/chem.201002589

Wakabayashi F.; Kondo J.N.; Domen K.; Hirose C. 1996, FT-IR Study of $H_2{}^{18}O$ Adsorption on H-ZSM-5: Direct Evidence for the Hydrogen-Bonded Adsorption of Water. J. Phys. Chem. 100 (5), 1442-1444. https://doi.org/10.1021/jp953089h

Wang L.; Zhang Z.; Yin C.; Shan Z.; Xiao F-S. 2010, Hierarchical mesoporous zeolites with controllable mesoporosity templated from cationic polymers. Microporous Mesoporous Mater. 131 (1-3), 58-67. https://doi.org/10.1016/j.micromeso.2009.12.001

Wang R.; Peng Z.; Wu P.; Lu J.; Rood M.J.; Sun H.; Zeng J.; Wang Y.; Yan Z. 2021, Direct Synthesis of Nanosheet-Stacked Hierarchical “Honey Stick-like” MFI Zeolites by an

Aromatic Heterocyclic Dual-Functional Organic Structure-Directing Agent . Chem. - Eur. J. 27 (34), 8694-8697. https://doi.org/10.1002/chem.202100701

Wang T.; Zhang L.; Wang H.; Yang W.; Fu Y.; Zhou W.; Yu W.; Xiang K.; Su Z.; Dai S.; Chai L. 2013, Controllable Synthesis of Hierarchical Porous Fe3O4 Particles Mediated by Poly(diallyldimethylammonium chloride) and Their Application in Arsenic Removal. ACS Appl. Mater. Interf. 5 (23), 12449-12459. https://doi.org/10.1021/am403533v

Xu D.; Feng J.; Che S. 2014, An insight into the role of the surfactant CTAB in the formation of microporous molecular sieves. Dalton Trans. 43 (9), 3612-3617. https://doi.org/10.1039/C3DT53308E

Yang G.; Wei Y.; Xu S.; Chen J.; Li J.; Liu Z.; Yu J.; Xu R. 2013, Nanosize-Enhanced Lifetime of SAPO-34 Catalysts in Methanol-to-Olefin Reactions. J. Phys. Chem. C 117 (16), 8214-8222 . https://doi.org/10.1021/jp312857p

Yu X.; Liu B.; Zhang Y. 2019, Effect of Si/Al ratio of high-silica HZSM-5 catalysts on the prins condensation of isobutylene and formaldehyde to isoprene, Heliyon 5 (5), E01640. https://doi.org/10.1016/j.heliyon.2019.e01640

Zhang Y.; Jin C. 2011, Rapid crystallization and morphological adjustment of zeolite ZSM-5 in nonionic emulsions. J. Solid State Chem. 184 (1), 1-6. https://doi.org/10.1016/j.jssc.2010.10.012

Zhao S.; Kim K.D.; Wang L.; Ryoo R.; Huang J. 2021, Tailoring Multiple Porosities of Hierarchical ZSM-5 Zeolites by Carbon Dots for High-Performance Catalytic Transformation. Adv. Mater. Interfaces 8 (4), 2001846, 1-7. https://doi.org/10.1002/admi.202001846

Zhou M.; Wang F.; Xiao W.; Gao L.; Xiao G. 2016, The comparison of mesoporous ZSM-5 zeolite catalysts prepared by different mesoporous templates and their catalytic performance in the methanol to aromatics reaction. Reac. Kinet. Mech. Cat. 119, 699-713. https://doi.org/10.1007/s11144-016-1076-8

Zhu J.; Zhu Y.; Zhu L.; Rigutto M.; van der Made A.; Yang A.C.; Pan S.; Wang L.; Zhu L.; Jin Y.; Sun Q.; Wu Q.; Meng X.; Zhang D.; Han Y.; Li J.; Chu Y.; Zheng A.; Qiu S.; Zheng X.; Xiao F-S. 2014, Highly Mesoporous Single-Crystalline Zeolite Beta Synthesized Using a Nonsurfactant Cationic Polymer as a Dual-Function Template. J. Am. Chem. Soc. 136 (6), 2503-2510. https://doi.org/10.1021/ja411117y

Zhu Y.; Hua Z.; Zhou J.; Wang L.; Zhao J.; Gong Y.; Wu W.; Ruan M.; Shi J. 2011, Hierarchical Mesoporous Zeolites: Direct Self-Assembly Synthesis in a Conventional Surfactant Solution by Kinetic Control over the Zeolite Seed Formation. Chem. - Eur. J. 17 (51), 14618-14627. https://doi.org/10.1002/chem.201101401

GRAPHICAL ABSTRACT